Journal of Applied Physics

Radiation-induced conductivity in polystyrene, a common insulating polymer with a hopping conduction

Cite as: J. Appl. Phys. **129**, 175107 (2021); https://doi.org/10.1063/5.0048649
Submitted: 25 February 2021 . Accepted: 16 April 2021 . Published Online: 05 May 2021

Andrey Tyutnev, Vladimir Saenko, Ilshat Mullakhmetov, and Ilya Agapov

AIP Publishing

Journal of Applied Physics ARTICLE scitation.org/journal/jap

Radiation-induced conductivity in polystyrene, a common insulating polymer with a hopping conduction

Cite as: J. Appl. Phys. **129**, 175107 (2021); doi: 10.1063/5.0048649
Submitted: 25 February 2021 · Accepted: 16 April 2021 ·
Published Online: 5 May 2021

Andrey Tyutnev,[a] Vladimir Saenko,[b] Ilshat Mullakhmetov, and Ilya Agapov

AFFILIATIONS

National Research University Higher School of Economics, 20 Miasnitskaya Ulitsa, Moscow 101000, Russia

[a]**E-mail:** aptyutnev@yandex.ru
[b]**Author to whom correspondence should be addressed:** saenko19@gmail.com

ABSTRACT

Radiation-induced conductivity (RIC) of polystyrene has been studied experimentally and numerically mostly in a small-signal regime in a broad time range from some nanoseconds to seconds. It has been established that hole transport is dispersive with a low value of the dispersion parameter $\alpha = 0.35$. We have suggested a direct method of determination of the frequency factor of the Rose–Fowler–Vaisberg model, which has been parameterized using computer simulations by the trial and error method. The main outstanding concern is the application of the Onsager theory of geminate recombination concerning the field dependence of the free carrier yield and the possible frequency factor increase at high electric fields. The effect of hopping transport on the RIC in this common insulating polymer is still to be understood.

I. INTRODUCTION

In our previous paper,[1] a new methodological approach to study the radiation-induced conductivity (RIC) in common insulating polymers has been suggested and successfully realized. Time-resolved measurements were made using a small-signal, step-function irradiation over a broad time interval from microseconds to several seconds. Experimental results for polyvinylcarbazole (PVK) and molecularly doped polymers (MDPs) could be rationalized within the traditional Rose–Fowler–Vaisberg (RFV) model[1,2] based on a quasi-band multiple trapping (MT) formalism based on an exponential trap distribution.[3–5] This approach proved unsatisfactory for polyimide (trademark Kapton) and Russian-made polyethyleneterephthalate (PET-1) for which a simple exponential trap distribution had to be replaced by a more complex aggregate distribution taking account of the presence of deep traps.[1] In this group of polymers, polystyrene (PS) stood in between tending to the PVK and MDP. We believe that a closer look at the RIC of PS may help to deepen our understanding of this complex phenomenon.

We will show that hole transport in PS is strongly dispersive, in highly non-equilibrium conditions, with the dispersion parameter $\alpha = 0.35$ so that the well-developed theory of anomalous charge carrier transport may be applied for data interpretation.[1,5] Also, we will see that PS unlike PVK is much more suitable for a direct assessment of one of the major parameters of the RFV model—the frequency factor and its field dependence, which is currently overlooked by the engineering community.

Model parameterization needs a well-established correlation between the dose rate and the carrier generation rate usually provided by the Onsager field-assisted thermal dissociation of the geminate electron–hole pairs.[6,7]

Hole drift mobility in PS has been known to be low[8–11] and the time-of-flight (TOF) technique so effective in studying charge carrier transport in photoconductive PVK and MDP[12] proved unsuccessful in PS, which lacks photoconductivity in the near UV region. Thus, ionizing radiation is the only experimental means presently available for studying hole transport in PS,[13] which presumably features a hopping conduction with benzene rings acting as hopping centers. In this respect, PS resembles PVK, a test-bed for studying hopping conductivity in disordered organics.[14] But, there arises a general question about validity of describing the hopping transport in terms of the quasi-band picture, for example, based on the MT formulation.[15]

Now, that experimental and numerical techniques have been recently upgraded,[1,16,17] we plan to perform controlled experiments

and fulfil numerical calculations to parameterize the RFV model for PS. Also, we would like to concern some ambiguities in the interpretation of the prompt component of the RIC in polymers with the hopping conduction.

II. EXPERIMENTAL

A. Methodology

In our studies like in Ref. 1, we used capacitor-grade, biaxially stretched PS films (Styroflex, 20 μm thick produced by NSW firm, FRG). Samples has been cut from the same band 100 mm wide with a shelf life of about 35 years, which is still at our disposal. Specimens (40 mm in diameter) were supplied with evaporated 50 nm Al electrodes, 32 mm in diameter. We used only *fresh* samples for each long-time irradiation run. Experiments have been conducted at room temperature and most data refer to an electric field of 4×10^7 V/m.

The ELA-65 electron gun provided 50 keV electrons falling normally upon a polymer sample. A shutter with an opening time of 0.08 s in long-time irradiations was covered with a conducting luminescent paint to visualize the irradiated spot. It was found that for a collimator 20 mm in diameter this spot was 30 mm in diameter well inside Al electrodes. The dose depth profile has been typical for 50 keV electrons so that an average dose rate R_0according to our Monte–Carlo simulations[18] was 1.7 times larger than at the sample's front surface. For the beam current of 1 nA (1 mV/1 MΩ) passing through a collimator, R_0 was estimated to be 1.6 Gy/s. RC time constant was less than 2% of the pulse length (further details are given in Ref. 1).

B. General phenomenology

An experimentally measured quantity is the RIC current density j_r. The raw data were processed to separate the delayed component j_{rd} from the total signal: $j_{rd} = j_r - j_p$ where j_p is the RIC prompt component.[1] In the case of the small-signal irradiation when an applied field is uniform and constant while a dose rate is uniform, it is useful to introduce normalized quantities: conductivity $\gamma_r = j_r/F_0$ and reduced conductivity $K_r = \gamma_r/R_0$ with natural separation into delayed and prompt components.

Our main interest concerns the delayed component that defines the transport properties of a polymer and is described by a theoretical model based on the MT approach (the RFV or RFVm models).[1] The reduced prompt conductivity K_p is a material parameter and needs only once to be determined.

Theoretical RIC response is computed on the whole time scale. Experimentally, this could be done only in separate time intervals with subsequent matching of data points at boundaries.

In our previous work[1] (see Fig. 3 in it), we plotted values of $K_{rd} = \gamma_{rd}/R_0$ at specified times and used a B-spline envelope of these data points as a probe for applicability of the RFV model. This envelope being close to a straight line over a long time like in PVK or low-density polyethylene (LDPE) testified in favor of this tendency. Roughly, PS also fitted this approach but in our later work,[17] we still resorted to the RFVm model for computer simulations of the hole transport in it.

In the RFV model,[13] an exponent $\beta = d\lg j_{rd}/d\lg t$ stays constant from tens of microseconds to some seconds and in this case, $\beta = \alpha$ (the dispersion parameter of the model). It is important that at long-time irradiations driving the RIC into recombination-controlled regime, one observes a power-like dependence of the maximum RIC on the dose rate R_0,

$$\gamma_{rm} \propto R_0^{\Delta}, \tag{1}$$

with $\Delta = (1+\beta)^{-1}$.

C. Experimental results

Our numerous results show that K_p is equal to $3.5 \times 10^{-15}\,\Omega^{-1}\,\mathrm{m}^{-1}\,\mathrm{Gy}^{-1}\,\mathrm{s}$ (±20%).[19] This value refers to 8- and 40 ns irradiations by 8 MeV electrons[19] but was reaffirmed on ELA-50 using triangular 3 μs pulses at low electric fields when RIC response was totally dominated by a prompt component.[16] The above value of K_p has been used in the present work for processing RIC curves.

The measured values of K_{rd} at fixed times are presented in Table I and as star conductivity points at a dose rate of 1.6 Gy/s in Fig. 1. Center stars refer to pulses ending at 20 μs and 1 ms, respectively, as in Ref. 1. Two far left points at 40 ns and 2 μs were obtained by processing our previous publications which will be analyzed in detail in Sec. III D.

Two vertical arrows show the dead zone of ELA-50 where irradiations could not be started or properly processed.[16] As for the far right data point with which we encountered a difficulty in Ref. 1, it will be discussed in Sec. III E.

It is important that the dotted straight line $j \propto t^{0.35}$ runs through all data points except the far left one which has also a good reason to divert as will be shown in Sec. III D.

It is important that Δ estimated from the long-time exposures (see formula 1) agrees with the above value of the exponent β. Thus, the application of the RFV model for the description of the RIC in PS seems to be justified.

III. RFV MODEL AND ITS PARAMETERIZATION

A. Problem formulation

The basic equations of the RFV model are well-known,[1,13]

$$\begin{cases} \dfrac{dN(t)}{dt} = g_0 - k_{rec} N_0(t) N(t) \\ \dfrac{\partial \rho(E,t)}{\partial t} = k_c N_0(t) \left[\dfrac{M_0}{E_1} \exp\left(-\dfrac{E}{E_1}\right) - \rho(E,t) \right] - \nu_0 \exp\left(-\dfrac{E}{kT}\right) \rho(E,t), \\ N(t) = N_0(t) + \int_0^{\infty} \rho(E,t)\, dE \end{cases} \tag{2}$$

where $N_0(t)$ and $\rho(E, t)$ are both zero at $t = 0$.

TABLE I. Experimentally determined values of K_{rd} (in units of $10^{-14}\,\Omega^{-1}\,\mathrm{m}^{-1}\,\mathrm{Gy}^{-1}\,\mathrm{s}$) taken in a small-signal regime at indicated times.

40 ns	2 μs	20 μs	1 ms	5.8 s
0.03	1.2	1.8	9.0	180

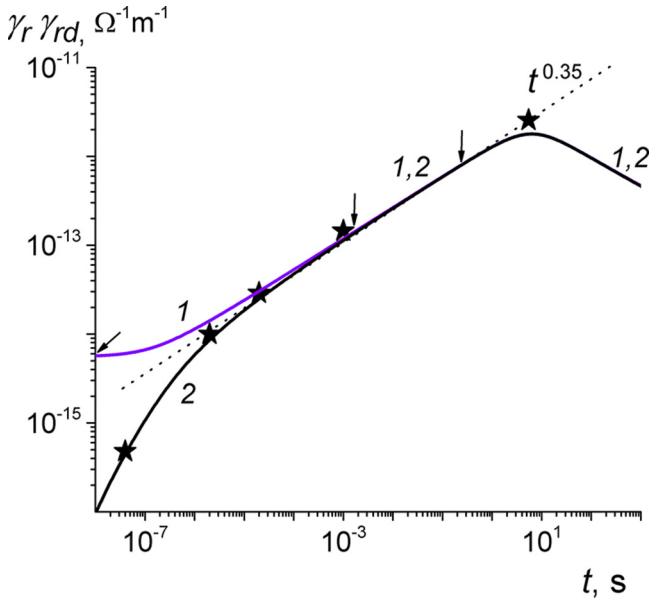

FIG. 1. Computed curve of the RIC according to RFV model parameters indicated in Table II (Sec. III E) best fitting experimental data points (stars) for the delayed component γ_{rd} (curve 2). Also shown is the total conductivity γ_r (curve 1) with its theoretical prompt component at early times ($5.7 \times 10^{-15}\ \Omega^{-1}m^{-1}$, indicated by an inclined arrow). All data refer to a dose rate 1.6 Gy/s ($g_0 = 10^{20}\ \mathbf{m^{-3}s^{-1}}$).

By definition, the RIC is $\gamma_r(t) = e\mu_0 N_0(t)$. Thus, system (2) refers to a unipolar conduction with only one sign carriers being mobile (in our case, holes). The oppositely charged carriers are immobile and act as recombination centers.

Here, $N(t)$ is the total concentration of radiation-produced holes (due to charge neutrality, equal to that of electrons). $N_0(t)$ is the concentration of holes in extended states (in the valence band) with the microscopic mobility μ_0; g_0 is the generation rate of free holes (assumed time and space independent during irradiation);k_{rec} is the recombination coefficient; k_c is the trapping rate constant; M_0 is the total concentration of traps distributed continuously in energy E (taken positive); $\rho(E, t)$ is the time dependent density distribution of trapped holes; ν_0 is the frequency factor; T is the temperature; k is the Boltzmann's constant, and e is the elementary electric charge. Also, $\tau_0 = (k_c M_0)^{-1}$ is the lifetime of mobile holes before trapping. Dispersion parameter $\alpha = kT/E_1$.

The second and third equations in system (2) are generic for a quasi-band description of the carrier transport in a dielectric with a unipolar (in our case, hole) conduction. The first equation (the continuity relation) in the present form describes a typical one-dimensional RIC problem ignoring any TOF effects. This form of system (2) plays is used in the present work for identifying RFV parameters. Changing properly the continuity equation and allowing $g_0 \to 0$, the TOF problem may be adequately treated as well.[1] Computer programs for both RIC and TOF experiments have been compiled and verified.[13]

B. Model parameterization

Model parameterization proceeds using recommendations given in our previous publications.[1,13] The fact that in our case $\alpha \leq 0.5$, makes the application of the analytic theory developed in Refs. 5 and 20 quantitatively accurate. It means that TOF-2 experiment (pulsed small-signal irradiation at low (RIC) and high (properly TOF-2)[1] field can be easily dealt with very accurately).

The charge carrier transport in the RFV model is characterized by four internal parameters $\alpha, \mu_0, \tau_{0.}, \nu_{.0}$ and one exterior parameter reflecting specifics of the interaction of ionizing radiations with matter $\eta_0 = g_0/R_0$connecting theory (g_0) with experiment (R_0). Theory of dispersive transport predicts that $\mu_0$and τ_0 enter all analytical formulas only as a product $\mu_0\tau_0$. More to that, in a small-signal regime for $\nu_0 t \gg 1$, one deals with a more complicated product $\varsigma = \mu_0\tau_0\nu_0^{\alpha}$ uniting all internal parameters.[1] The existing analytical formulas may be used for preliminary selection of parameter values. Especially valuable is the general analytic formulation for MathCad calculations (taking less than a second) of both small-signal RIC and TOF-2 experimental setups.[1,20]

C. Carrier generation rate

It is known that half of the absorbed energy during irradiation of condensed matter (liquid or solid) is immediately expended on ionization of molecules producing approximately three electron–hole pairs per 100 eV of absorbed energy, the other part being lost on excitation but finally they all degrade into thermal energy. Thus, the total radiation yield of charged species $G_i \approx 3$. This figure is rather common for crystal and amorphous solids. At this early time (10^{-16} s), the spatial distribution of charged species is highly non-homogeneous (isolated and overlapping geminate pairs and ionic groups). Somewhat later (10^{-12} s), there starts a reorganization process including an initial recombination and spatial spreading of epithermal electrons. Finally, thermalization of all charged species completes and only isolated geminate pairs randomly oriented and homogeneously distributed in space are left in the system.[21]

From that moment, the irradiated system is readily treated in terms of the ordinary rate equations if the generation rate of free electrons is defined through $G_{fi} = fG_i$, where $f$is the free carrier escape probability given by the Onsager theory.[6,7] In its conventional form, the electron–hole distance in a geminate pair $r_0$is assumed to be constant thus greatly simplifying an analysis.[22,23]

Quantitative investigations of the radiation free career yields $G_{fi}(F_0)$ have been extensively pursued in dielectric liquids (see reviews).[7,24] In linear hydrocarbons like n-hexane, a typical value of parameter r_0 was 6 nm but in some liquids with exceptionally high electron mobility (about 10 cm^2/V m) this parameter approached 100 nm. Nothing of the kind could be observed in solids.

Even in crystalline anthracene (electron mobility about 1 cm^2/V m), the free carrier yield in pulsed x-ray irradiated anthracene crystals was found to be only $G_{fi} = 0.03$ ($f = 0.01$) at 4×10^6 V/m.[25] In disordered PVK, $r_0 \approx 6.3$ nm,[26] while in PET ($r_0 \approx 3.5$ nm)[27] and in PS G_{fi} could be expected to be even lower.[28] In Ref. 29, it has been shown that $G_i \approx 3$ in PS at an applied electric field of 2.5×10^8 V/m while in PET the same result has been registered at slightly lower field of 1.5×10^8 V/m.[30]

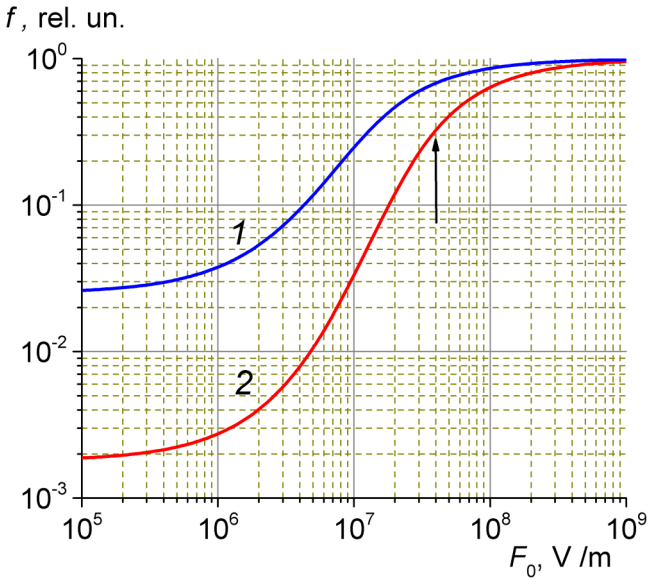

FIG. 2. Calculated curves of the free carrier escape probability as a function of the applied electric field according to the simplified Onsager model.[22,23] $r_0 = 6$ (1) and 3.5 nm (2). Relative dielectric constant $\varepsilon = 2.6$ (PS), room temperature. Arrow indicates the field 4×10^7 V/m.

Figure 2 shows f as a function of F_0 in PS for two most frequently cited values of r_0. At small fields, the curves strongly divert but tend to unity as an electric field goes to infinity. The curves markedly differ in maximum logarithmic slopes which happen at a field about 10^7 V/m amounting to unity (1) and 1.8 (2).

In this critical situation concerning the free carrier radiation yields, we had to use high electric fields to minimize the uncertainty due to the escape probability. At the chosen field of 4×10^7 V/m, we find from the above figure that $f = 0.68$ (curve 1) and 0.3 (2) leading to $G_{fi} = 2.0$ (1) and 0.9 (2), respectively.

The general expression relating the carrier generation rate $g_0(\mathrm{m^{-3}\,s^{-1}})$ to the dose rate R_0 (Gy/s) is as follows:

$$g_0 = 6.24x10^{19}\,\rho G_{fi} R_0, \tag{3}$$

where ρ is the polymer density (for PS, 1.06 g/cm^3). Calculations show that even at a high electric field of 4×10^7 V/m, there exists a noticeable scatter of data for the separation probability. In these circumstances, we had to make a choice and finally, we chose $G_{fi} = 1$. Then, for a dose rate 1.6 Gy/s, the carrier generation rate would be 10^{20} m^{-3} s^{-1}. Remembering that G_{fi} could be two times larger, we introduced the necessary parameter changes into Table II (these changes concern mainly τ_0 and slightly k_{rec} to accommodate specifically long-time irradiations).

D. Frequency factor

As early as in 1986,[19] we fulfilled an extended analysis of the current decay after pulsed excitation specifically in common polymers (as an example, LDPE) in terms of the RFV model under conditions when $\nu_0\tau_0 \ll 1$ that are typical for them. Numerical calculations have shown that in such circumstances decay transients form a plateau starting from just a pulse end and extending to a knee which marks beginning of a current decay in a dispersive regime following a power law $j \propto t^{-1+\alpha}$. The length of the plateau (we called it an initial mobility plateau) is approximately equal to ν_0^{-1}.

TABLE II. RFVm parameters for PS ($g_0 = 10^{20} m^{-3} s^{-1}$ at 4×10^7 V/m).

Parameter	α	$10^5 \times \mu_0$ m^2/V s	$10^{11}\,\tau_0$ (s)	$10^{-6}\,\nu_0$ (s^{-1})	$10^{14} k_{rec}$ (m^{-3} s^{-1})
G_{fi}					
1.0	0.35	1.0	3.5	8	6.9
2.0	0.35	1.0	1.75	8	6.9

At that time, our main interest was the general laws of RIC currents under pulse irradiations and in strong electric fields, frequency factor was considered as a fitting parameter. By the time, we first seriously took up the problem of direct determination of the frequency factor (2018),[31] high energy electron accelerators for ns-and μs- pulses were long not available for laboratory practice in Russia. In this situation, we employed an unprocessed data from our previous papers[32,33](Fig. 3).

Curve 2 on Fig. 3(a) demonstrates that the current decay after a pulse end in the pulse-time scale decreases very slowly forming a clear-cut plateau like it happened with LDPE at the end of a 2 μs pulse (see Fig. 1 in Ref. 33): it is quite understandable as ν_0 in LDPE is an order of magnitude smaller (in PS $\nu_0 = 8 \times 10^6$ s^{-1} while in LDPE it is 5×10^5 s^{-1}). The same curve represented by data points in Fig. 3(b) (pulse length increases to 2 μs) loses its plateau-like form and one needs a careful analysis to confirm the previous result ($\nu_0 \approx 8 \times 10^6$ s^{-1}).

Curves 1 and 2 in Fig. 3(a) clearly demonstrate that frequency factor depends on the electric field at least at these high fields. According to Ref. 32, increase of F_0 from 0.5 MV/m curve (2) to 1.6 MV/m curve (1) increases ν_0 by almost eight times.

The same change-over should exist on the build-up stage of $j_{rd}(t)$ during the pulse itself, but the RIC prompt component completely masks it. Only numerical calculations [Fig. 3(c)] reveal the real situation. Indeed, at the earliest times $j_{rd} \propto t$ (curve 2) but later on ($\nu_0 t \geq 1$) linear relationship break down and the current density starts to rise as a power law $j_{rd} \propto t^{\alpha}$(the same curve at $t \geq 0.5\mu s$). Note that curve 3 on plate 3c represents curve 2 on plate 3a on a logarithmic scale. It is also clear that the pulse length 20 μs used in the present study is too long for frequency factor determination.

In processing the above data, we heavily relied on the fact that the decay part of the RIC curve was plotted in the presence of a much larger but well-defined prompt component (see dashed vertical lines at 40 ns and 2 μs on plate 3c). This circumstance allowed us to assess K_{rd} values at 40 ns and 2 μs and to include them in Table I.

E. Recombination regime

Small-signal irradiation in the long run inevitably leads to a recombination-limited regime. Our irradiation facility ELA-50

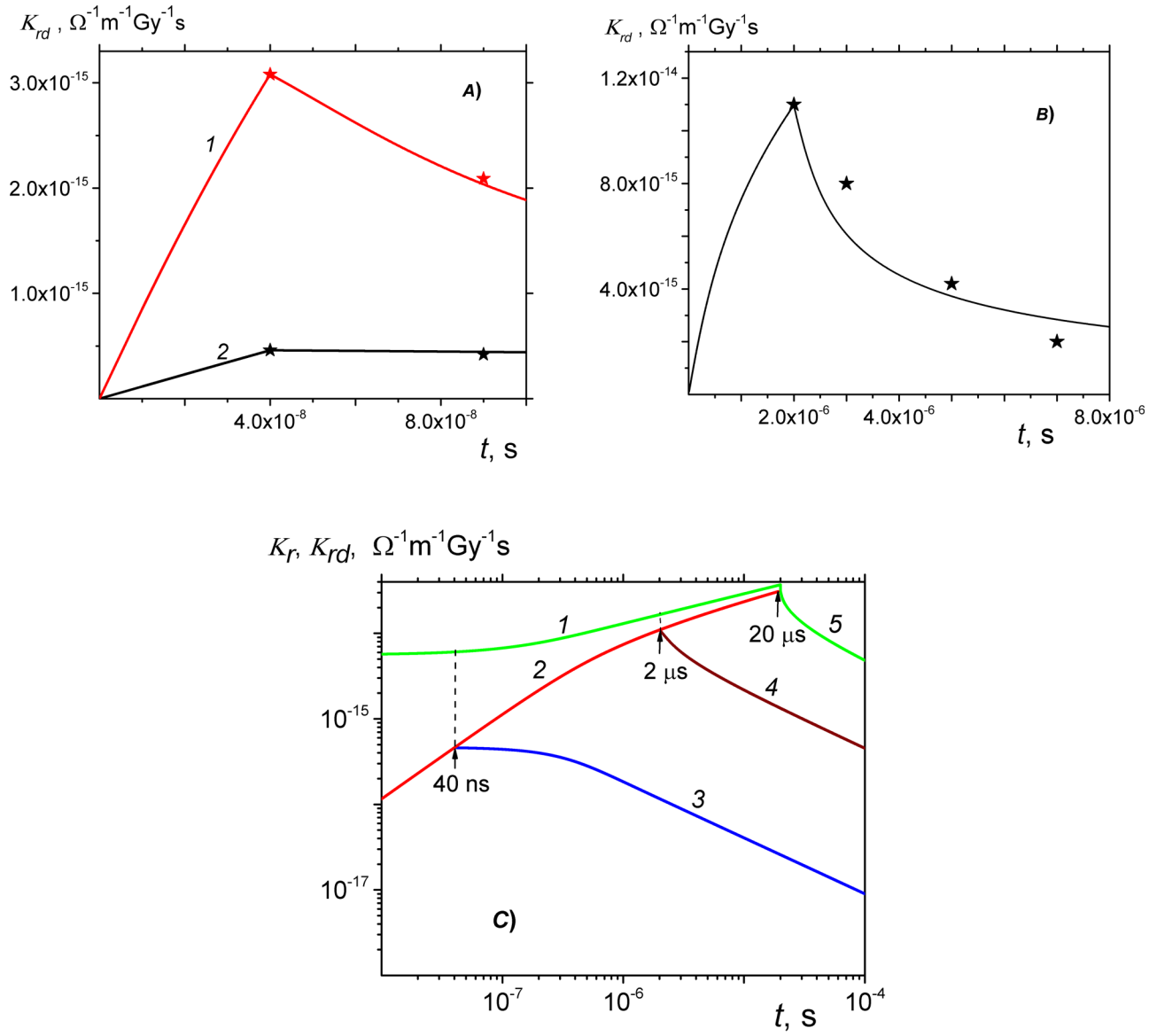

FIG. 3. Dispersive calculated curves ($\alpha = 0.35$ and $\nu_0 = 8 \times 10^6 s^{-1}$) used for approximate determination of the value of ν_0 in PS by comparing experimental data and calculated curves. Stars on plates A and B are selected data points from unprocessed figures from Refs. 32 and 33. Plate C shows separate development of both RIC components ($K_r(1)$ and $K_{rd}(2 - 5)$ for three pulse lengths (40 ns, 2, and 20 μs). For details, see text.

allows the smallest controlled dose rate 1.6 Gy/s) and we reach the RIC maximum at about 5 s (just outside the dead interval for small-signal irradiations indicated in Fig. 1). So to find a small-signal data point in line with other measurements on Fig. 1, we used well-known features of the RFV theory.[5,34] For this purpose, one computes a series of RIC transients for $\alpha = 0.35$ and $\nu_0 = 8 \times 10^6\ s^{-1}$ (other parameters may be taken from Table II) for a number of generation rates differing in decades (as in Fig. 4).

Now, at the time of a current maximum of γ_{rm} on 3, we find that the ratio of a point on curve *1* and γ_{rm} is equal to 1.45 as for any other curve in Fig. 4. In this way, one readily finds a data point at 5.4 s in the 1–10 s time interval in Fig. 1 as the far right star. Unfortunately, we overlooked this technique in our previous work.[1]

Now, Fig. 1 shows that starting from about 2 μs, the RICd build-up proceeds as a power function of time $j_{rd} \propto t^{0.35}$ until recombination limits it by forming a maximum on the current transient, in full accordance with the laws of the dispersive

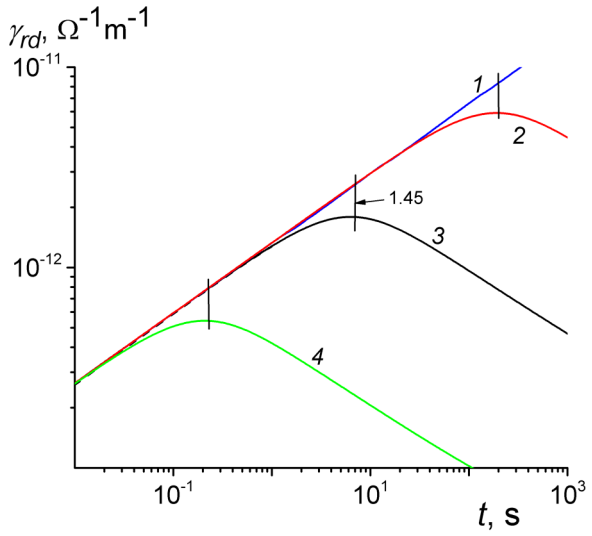

FIG. 4. Reduced RICd transients ($\alpha = 0.35$) computed for different carrier generation rates g_0: 10^{14} (1), 10^{18} (2), 10^{20} (3) and $10^{22}\,m^{-3}s^{-1}$ (4). Every curve was multiplied by a factor $10^{20}/g_0$ (curve 3 is given to scale and refers to a dose rate 1.6 Gy/s). For details see text.

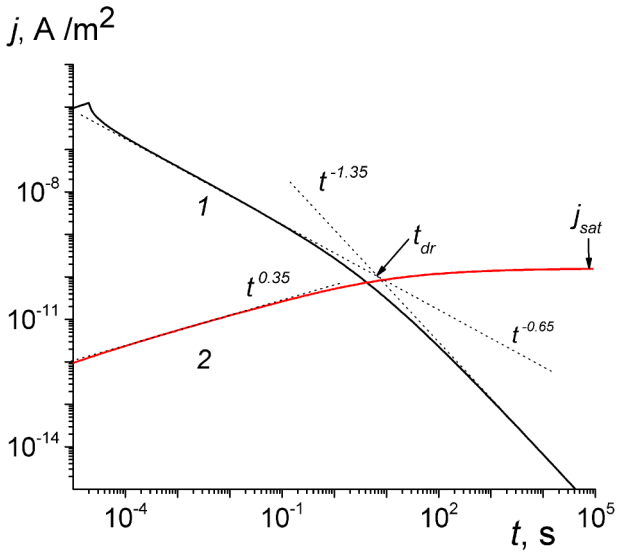

FIG. 5. Calculated TOF-2 (*1*) and dispersive transient (*2*) ($\alpha = 0.35$) under continuous irradiation for the RFV model with parameters given in Table II. Intersection of the pre-flight part ($j \propto t^{-0.65}$) with the post-flight part ($j \propto t^{-1.35}$) of the curve *1* marked by an arrow is the time of flight (7.13 s). Film thickness 20 μm, electric field 4×10^7 V/m, pulse length 20 μs (*1*). Carrier generation rate 10^{20} (*1*) and $10^{14}\,m^{-3}s^{-1}$ (*2*). Bulk recombination neglected in both cases.

transport. There are some inconsistencies in $K_{rd}(t)$behavior at early times as well but they should be ascribed to the influence of the frequency factor as it has already been explained in the preceding section.

F. TOF effects

Now, using RFV parameters from Table II, we can analyze two related types of small-signal uniform-excitation experiments. The first one is a conventional TOF-2 setup (Fig. 5, curve 1), while the second depicts the current build-up with a constant career generation rate in the absence of recombination (Fig. 5, curve 2). Owing to a small value of αin PS, accurate graphical determination of the transit time is almost impossible. Even in the case of numerical data (as in Fig. 5), we found that it is only about 6–8 s with theoretical prediction 7.13 s (see Ref. 17, formula 8). According to our numerical calculations drift mobility of holes in a PS film 20 μm thick 4×10^7 V/m is expected to be $7 \times 10^{-14}\,m^2/Vs$.

Published data favor drift mobility about $10^{-14}\,m^2/V\,m$ at high fields (see Sec. IV B). An important observation is that an asymptotic current decay is close to power law $t^{-1.3} - t^{-1.4}$ in accordance with the RFV theory. In the case of PS, the TOF measurement would not in any way help in determining G_{fi} as it was with PVK.[35]

Curve 2 in Fig. 5 is a build-up curve at continuous irradiation with $g_0 = \text{const}$. There is one interesting feature about transit time t_{dr}. On curve 1, it signals the moment when the current density suddenly increases its decay rate while on curve 2, it denotes the time from which the log slope $\beta = d\lg j/d\lg t$ starts to diminish to zero as $t \to \infty$ and the current density reaches its saturation value. We see that this process lasts for no less than 10^5 s.

The saturation current density is generation-controlled rather than transport-controlled entity and is equal to

$$j_{sat}(A/m^2) = 0.5\, g_0 Le, \tag{4}$$

where factor 1/2 accounts for a one-type (hole only) conduction. In high voltage experiments, one must be careful not to step over the boundary dividing the transport-controlled (for example, by the RFV model) current densities from the saturation curves which are parameter independent. In our case, the saturation current density is equal to $1.6 \times 10^{-10}\,A/m^2$ (indicated by a vertical arrow in Fig. 5). As indicated earlier, saturation current densities are generation-controlled quantities.

IV. DISCUSSION

A. Hopping nature of the hole transport in PS

As a polymer with hopping conduction, PS should be compared with another such polymer, PVK. In both polymers, the concentrations of branched molecular groups (phenyl rings in the former and carbazole groups in the latter) are very high 6.0 and $3.8 \times 10^{27}\,m^{-3}$, respectively. Ionization potentials of macromolecules differ considerably (in vacuum 8.8 vs 7.6 eV) which explains the fact why PVK is photoconductive, while PS is not. Note that PVK is much more heat resistant than PS (glass transition temperatures being 150 and 90 °C, respectively).

The radiation-related properties of PVK, this classical disordered organic solid, such as a drift mobility and its field dependence, the Onsager geminate recombination and free carrier radiation yield and the RIC and its parameterization could be found in our work.[35] First RIC experiments with PVK revealed its large RICd compared with ordinary polymers, $\alpha \geq 0.6$ and a readily observed TOF effects (see Ref. 35). All these questions relating to PS are only started to be studied in detail.

It is remarkable that the RICd in PVK[1,35] or MDP[36,37] can be correctly described in terms of the RFV model (or more generally, in the context of the MT formalism) without using labor- and time-consuming Monte–Carlo simulations.[38,39] This is in full accordance with the contemporary approach of the effective transport level which allows to reduce the hopping conduction to the quasi-band description with an acceptable level of confidenc.[40–43]

The role of the hopping centers in carrier transport is clearly seen in PVK and PS. Fortunately, mobility of electrons and holes have been studied in single crystals of N-isopropylcarbazole[44] and benzene,[45] the branching molecular groups acting as hopping centers in PVK and PS, respectively. In both crystals, electrons were somehow more mobile than holes by a factor of 3 and almost 10, respectively, with electron mobility being about 1 cm^2/V s. To understand the drastic difference in transport properties of PVK and PS, one should rely on quantum-mechanical analysis of the hopping transfer rates, if only on the level employed earlier in Ref. 46 when it was used to evaluate the effect of molecular rotations on the charge transfer between disordered carbazole groups in PVK.

One interesting question concerns the prompt conductivity in substances with a hopping conduction. It is expected that relaxation of excess charge carriers, introduced instantly into the spatially and energetically disordered distribution of hopping centers, proceeds according to the law $j \propto (\lg \nu_h t)/t$ and the time to complete it is about $\nu_h^{-1} \lg (E_{av}/kT)$ where ν_h is the jump frequency and E_{av} is the energy parameter of the energetical distribution.[47–49] This quantity simulates τ_0 in the MT formalism. After thermalization, excess charge carriers start multiple trapping process in both conduction types leading to similar current transients. Analysis is much simpler in the quasi-band model and that is why it was and still is the preferred instrument in the RIC engineering practice.

Frequency factor ν_0(a constant) entering the second equation in system (2) defines the rate of thermal release of holes captured by traps with the trapping energy E. Their transport proceeds via the valence band. In hopping conduction, one deals with hopping centers and hole transport occurs by jumps between them, the rate of this process depending on the energy difference and the distance between them. Theory predicts that generated holes will separate into two fractions, the minor one occupying energy states slightly higher than the center of the Gaussian energy distribution while the majority of holes will reside in much higher states. From now on, the hole transport starts to resemble the MT one.

From now on, the hole transport starts to resemble the MT one.

The mobility edge $E_C$becomes an effective transport level while the frequency factor gets equal to

$$\nu_0 = \Gamma_0 \exp(-2\gamma a_0 + E_C/kT) \quad (5)$$

where Γ_0 is the typical phonon frequency, γ is the inverse localization radius, and a_0 is a typical hopping distance. Also, one needs to know rms $\sigma$of the site energy distribution and temperature which enter parameters E_C and a_0.[41] These data are known mostly for model systems,[40–43] but not for technical polymers like PS.

B. Outstanding problems of the RIC in polymers

A serious problem in radiation physics of insulating polymers and RIC in them, continues to be an evaluation of the field dependence of the free career yield G_{fi} and an average distance between sibling charges in a geminate pair. Full scale measurements encounter formidable difficulties even in crystalline solids,[25,50,51] let alone low-mobility polymers in which charge collection in reasonable times is questionable. Another approach to probe G_{fi} field dependence is studying the variation of the current decay with increasing applied field under conditions of a small-signal pulsed irradiation and a minimum variation of the asymptotic current decay form (Fig. 6).

First of all, we note that only the build-up of a current density of the delayed component ($K_{rd} = K_r - K_p$ which is represented by curve *1*a) follows the law $j_{rd} \propto t^{0.35}$ while the RIC approaches this build-up law only at very high fields (upper curves). This procedure is well illustrated in Figs. 1 and 3(c) for a pulse length of 40 ns. Specifically, for LDPE this procedure was presented in Fig. 4(a) in Ref. 1.

According to the theory of a dispersive transport (see preflight part of curve 1 in Fig. 5), the expected current decay should be close to $t^{-0.65}$ but we never saw this: at low fields, it

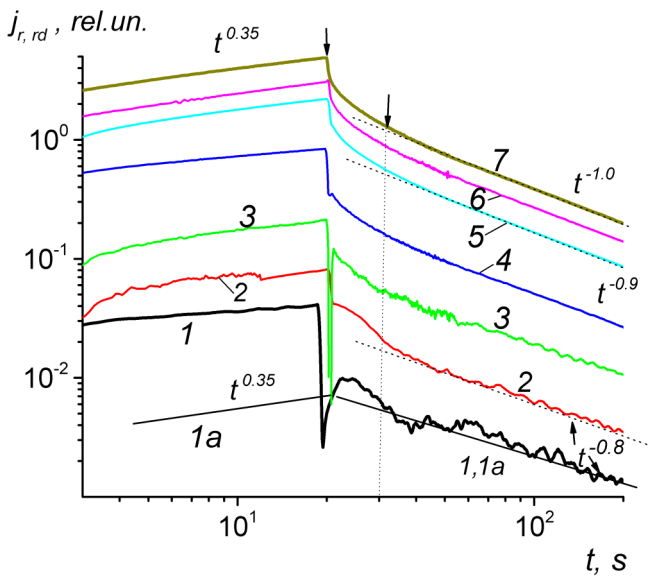

FIG. 6. Experimental TOF-2 current transients measured across 100 Ω resistor (RC < 0.2 μs) and plotted in logarithmic coordinates. Voltage: 50 (*1,1a*), 100 (*2*), 200 (*3*), 400 (*4*), 800 (*5*), 1000 (*6*) and 1200 V (*7*). Film thickness 20 μm, dose rate 3.6×10^5 Gy/s, pulse length 20 μs. At small voltages less than 300 V signals are rather noisy.

demonstrated the slowest rate of decay $t^{-0.80}$ increasing it again to $t^{-1.0}$ at times which are much shorter than the time of flight of 7.1 s, contrary to the behavior observed in PVK.[1,35] At present, this is still a serious problem waiting for its explanation.

To study the field dependence of the free carrier generation yield (if only in relative units), we measured RICd current transients at the pulse end and 10 μs afterwards as indicated by two vertical arrows (Fig. 6). The field range covered in these investigations extended from 2.5×10^6 to 6×10^7 V/m (Fig. 7). Our data (filled and open circles) group around a theoretical prediction of the Onsager theory for $r_0 = 6$ nm (down triangles) based on processed curve 1 from Fig. 2.

Data points of j_{rd}/F_0 measured at the pulse end are typically higher than those taken 10 μs afterwards. The expected rise of G_{fi} in the above field range for $r_0 = 6$ nm (see Fig. 2) is close to 9.6 (the rise of the ratio j/F_0 in the same field range for filled circles is about 20). The upward deviation of these symbols compared with down triangles at high fields may be partly due to the field dependence of the frequency factor (see Fig. 3(a) and Ref. 32 for more extended discussion).

Note that stars run substantially lower than even open circles. It is important that up triangles, even under restrictions of Fig. 7, run contrary to experiment. In the field range used, G_{fi} is predicted to rise for more than 100 times (see curve 2 in Fig. 2). Our data clearly prefer data for $r_0 = 6$ nm (as in PVK),[26,35] but not 3.5 nm (as in PET).[27]

Maeda[30] in response to Hughes[27] results reporting $r_0 = 3.5$ nm in PET (trademark Mylar) made extensive investigations on PET and published it as a short note.

Following Hughes, authors of Ref. 30 used the steady-state current at long-time small-signal irradiations (reached at first seconds after its start) as a relative measure of the free carrier yield. Using 6 μm films, they established that the total carrier yield was close to 3.0 at 1.8×10^8 V/m. On the other hand, working with a 50 μm films, they found that the rise of the ratio j/F_0 amounted only to 5.5 times in the field range of 10^6–10^8 V/m (stars in Fig. 7). This discrepancy may be attributed to the fact that their method effectively excluded the influence of the rising drift mobility (frequency factor) in high electric fields on the steady-state current since it was a generation-controlled current while we measured the transport dependent one. The authors refrained from any comments on r_0- dilemma ignited by Hughes' work.[27]

Working at very high electric fields ($\geq 10^8$ V/m) with small-signal long-time irradiations, one should be careful about interference of the secondary hole-injection currents from certain electrodes (for example, gold).[29,30]

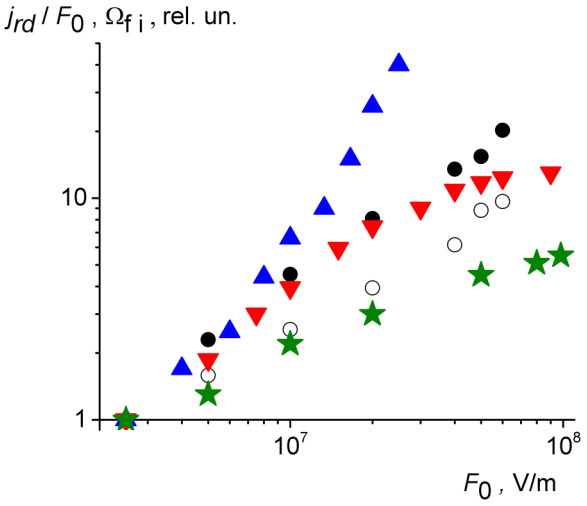

FIG. 7. Field dependence of the ratio j_{rd}/F_0 taken at pulse end (filled circles) and 10 μs afterwards (open circles) from Fig. 6, but also of the ratio j_{st}/F_0 given in Ref. 30 on Fig. 2 (stars) together with two theoretical curves $G_{fi}(F_0)$ taken from Fig. 2 for $r_0 = 6$ (down triangles) and 3.5 nm (up triangles). All data was normalized at a field strength of 2.5×10^6 V/m.

B. Hole mobility

PS is a low-mobility common insulating polymer and the general situation in this field has been recently discussed in[17] and it was placed in a group of polymers defying the RFV model whose mobility was explained using the RFVm model. For PS, we had to make a concession by approximating TOF-2δ^1 curve with a conventional dispersive curve with $\alpha = 0.3$. According to numerical calculations drift mobility of holes in a PS film 20 μm thick 4×10^7 V/m is expected to be 7×10^{-14} m^2/V s.

The most reliable measurement of the hole mobility in PS has been done in Ref. 52. The author used in fact a variant of the TOF-2 method: irradiation time 0.3 s, electron energy 4 keV, current density 3 nA/cm^2, and electric field 4×10^7 V/m. Unfortunately, measurements were made at 333 K or higher. Even at 333 K, the mobility was only 10^{-14} m^2/V s, but the post flight decay followed an algebraic law $t^{-1.6}$. Electron mobility was negligibly small.

Reference 11 reported controversial results. At room temperature, mobilities of hole and electrons were almost equal and rather high (3×10^{-9} m^2/V s) at 4×10^7 V/m. In our previously published paper,[53] we found that hole mobility at room temperature was about 10^{-13} m^2/V s even at 2×10^8 V/m with post-flight curve running as $t^{-1.35}$ if only approximately.

V. CONCLUSIONS

We have shown that the RFV model can be used for description of the RIC in PS and we used it to parameterize it with the only uncertainty about a factor of two concerning the link between the free carrier rate g_0 and the dose rate R_0 at a field 4×10^7 V/m. For the first time, the frequency factor, an important RFV model parameter, has been found for PS directly from experiment and have been shown to be approximately equal to 8×10^6 s^{-1}. Our data for a field dependence of decay currents after pulsed excitations show that an electron–hole separation r_0 in an isolated geminate pair is more likely to be 6 nm (as in PVK) rather than 3.5 nm as reported earlier by Hughes for PET.

Drift mobility of holes in PS at room temperature still needs a careful examination at high electric fields. PS is a polymer with hopping (hole) conductivity and like PVK should be analyzed in terms of the quasi-band RFV model as is the case with all other

insulating polymers since numerical calculations using the quasi-band approach are much more effective in the engineering practice than the Monte–Carlo computer simulations. In conventional dispersive transport, there is the following relation between α and the exponent β_1 describing the asymptotic current decay in the small-signal regime$j \propto t^{-\beta_1}$: $\beta_1 = (1 - \alpha)$. Preliminary results have shown that experimental value of β_1 (0.8–1.0), disagrees with the theoretical expectation value 0.65 as Fig. 6 demonstrates. This observation contradicts the RFV model but in view of the vast information supporting it, the above result certainly needs further careful investigation.

ACKNOWLEDGMENTS

The authors are indebted to the Basic Research Program of the National Research University Higher School of Economics, Moscow, for their support.

DATA AVAILABILITY

The data that support the findings of this study are available from the corresponding author upon reasonable request.

REFERENCES

[1]A. P. Tyutnev, V. S. Saenko, R. S. Ikhsanov, and E. A. Krouk, J. Appl. Phys. **126**, 095501 (2019).
[2]G. S. Mingaleev, A. P. Tyutnev, B. P. Gerasimov, and I. A. Kulchitskaya, Phys. Status Solidi A **93**, 251 (1986).
[3]V. D. Lakin, L. Marks, and J. Noolandi, Phys. Rev. B **15**, 5834 (1977).
[4]T. Tiedje and A. Rose, Solid State Commun. **37**, 49 (1981).
[5]V. I. Arkhipov, M. S. Iovu, A. I. Rudenko, and S. D. Shutov, Phys. Status Solidi A **54**, 67 (1979).
[6]L. Onsager, Phys. Rev. **54**, 554 (1938).
[7]A. Hummel, Adv. Rad. Chem. **4**, 1 (1974).
[8]E. H. Martin and J. Hirsch, Solid State Commun. **7**, 279 (1969).
[9]E. H. Martin and J. Hirsch, J. Appl. Phys. **43**, 1001 (1972).
[10]Y. Suzuoki, T. Mizutani, and M. Ieda, Japan. J. Appl. Phys. **15**, 1665 (1976).
[11]J. Kyokane, S. Harada, K. Yoshino, and Y. Inuishi, Japan. J. Appl. Phys. **18**, 1479 (1979).
[12]P. M. Borsenberger and D. S. Weiss, *Organic Photoreceptors for Imaging Systems* (Marcel Dekker, New York, NY, 1993).
[13]A. P. Tyutnev, V. S. Saenko, E. D. Pozhidaev, and R. S. Ikhsanov, IEEE Trans. Plasma Sci. **43**, 2915 (2015).
[14]H. Bässler, Phys. Status Solidi B **107**, 9 (1981).
[15]I. P. Zvyagin, Phys. Status Solidi B **95**, 227 (1979).
[16]A. P. Tyutnev, V. S. Saenko, A. D. Zhadov, and E. D. Pozhidaev, Polymers **11**, 2061 (2019).
[17]A. Tyutnev, R. Ikhsanov, V. Saenko, and V. Ashmarin, J. Appl. Phys. **128**, 225501 (2020).
[18]A. P. Tyutnev, D. N. Sadovnichii, V. S. Saenko, and E. D. Pozhidaev, Polym. Sci. A **47**, 1174 (2005).
[19]A. P. Tyutnev, V. N. Abramov, P. I. Dubenskov, V. S. Saenko, A. V. Vannikov, and E. D. Pozhidaev, Acta Polym. **37**, 336 (1986).
[20]V. R. Nikitenko, A. P. Tyutnev, V. S. Saenko, and E. D. Pozhidaev, Khim. Phizika **23**, 92 (2004) (in Russian).
[21]*Kinetics of Non-Homogeneous Processes*, edited by G. R. Freeman (Wiley, New York, NY, 1987).
[22]K. M. Hong and J. Noolandi, J. Chem. Phys. **68**, 5163 (1978).
[23]D. M. Pai and R. C. Enck, Phys. Rev. B **17**, 5163 (1975).
[24]A. Hummel and W. F. Schmidt, Radiat. Res. Rev **5**, 199 (1974).
[25]R. G. Kepler and F. N. Coppage, Phys. Rev. **151**, 610 (1966).
[26]R. C. Hughes, IEEE Trans. Nucl. Sci. **18**, 281 (1971).
[27]R. C. Hughes, in *Proceedings of 2nd International Conference on Electrophotography*, Washington, DC, 24–27 October 1975 (1975), pp. 147–151.
[28]F. N. Coppage and R. G. Kepler, IEEE Trans. Nucl. Sci. **13**, 227 (1966).
[29]H. Maeda, M. Kurashige, and T. Nakakita, J. Appl. Phys. **50**, 7247 (1979).
[30]H. Maeda, M. Kurashige, D. Ito, and T. Nakakita, Appl, Phys. Lett **32**, 278 (1978).
[31]A. P. Tyutnev, V. S. Saenko, and E. D. Pozhidaev, IEEE Trans. Plasma Sci. **46**, 645 (2018).
[32]A. P. Tyutnev, B. L. Linetskii, A. V. Nikerov, and V. S. Saenko, Russ. J. Phys. Chem. B. **9**, 648 (2015).
[33]A. P. Tyutnev and D. N. Sadovnichii, Chem. Phys. Reports **17**, 587 (1998).
[34]V. I. Arkhipov, Y. A. Popova, and A. I. Rudenko, Phil. Mag. B **48**, 401 (1983).
[35]A. P. Tyutnev, V. S. Saenko, E. D. Pozhidaev, and V. A. Kolesnikov, J. Phys. Condens. Matter **18**, 6365 (2006).
[36]A. P. Tyutnev, V. S. Saenko, and E. D. Pozhidaev, Chem. Phys. **415**, 133 (2013).
[37]A. P. Tyutnev, D. S. Weiss, D. H. Dunlap, and V. S. Saenko, J. Phys. Chem. C **118**, 5150 (2014).
[38]H. Bässler, Phys. Status Solidi B **175**, 15 (1993).
[39]S. V. Novikov, D. H. Dunlap, V. M. Kenkre, P. E. Parris, and A. V. Vannikov, Phys. Rev. Lett. **81**, 4472 (1998).
[40]S. D. Baranovskii, Phys. Status Solidi A **215**, 1700676 (2018).
[41]V. R. Nikitenko and M. N. Strikhanov, J. Appl. Phys. **115**, 073704 (2014).
[42]V. R. Nikitenko, A. Y. Saunina, A. P. Tyutnev, and O. V. Prezdo, J. Phys. Chem. C **121**, 7776 (2017).
[43]M. D. Khan, V. R. Nikitenko, A. P. Tyutnev, and R. S. Ikhsanov, J. Phys. Chem. C **123**, 1653 (2019).
[44]J. H. Sharp, J. Phys. Chem. **71**, 2587 (1967).
[45]H. Hirth and F. Stöckmann, Phys. Status Solidi B **51**, 691 (1972).
[46]J. H. Slowik and I. Chen, J. Appl. Phys. **54**, 4467 (1983).
[47]N. I. Chekunaev and V. N. Fleurov, J. Phys. C: Solid State Phys. **17**, 2917 (1984).
[48]D. Monroe, Phys. Rev. Lett. **54**, 146 (1985).
[49]A. P. Tyutnev, A. V. Subbotin, and N. I. Chekunaev, Khimiya, Vysokikh Energ. **22**, 338 (1988) (in Russian).
[50]R. R. Chance and C. L. Braun, J. Chem. Phys. **59**, 2369 (1973).
[51]R. R. Chance and C. L. Braun, J. Chem. Phys. **64**, 3573 (1976).
[52]S. A. Khatipov, High Energy Chem. **35**, 291 (2001).
[53]V. N. Abramov, E. D. Pozhidaev, A. P. Tyutnev, V. S. Saenko, and A. V. Vannikov, Polym. Sci. USSR **29**, 285 (1987).